

REPORT DOCUMENTATION PAGE				<i>Form Approved</i> OMB No. 0704-0188	
Public reporting burden for this collection of information is estimated to average 1 hour per response, including the time for reviewing instructions, searching existing data sources, gathering and maintaining the data needed, and completing and reviewing this collection of information. Send comments regarding this burden estimate or any other aspect of this collection of information, including suggestions for reducing this burden to Department of Defense, Washington Headquarters Services, Directorate for Information Operations and Reports (0704-0188), 1215 Jefferson Davis Highway, Suite 1204, Arlington, VA 22202-4302. Respondents should be aware that notwithstanding any other provision of law, no person shall be subject to any penalty for failing to comply with a collection of information if it does not display a currently valid OMB control number. PLEASE DO NOT RETURN YOUR FORM TO THE ABOVE ADDRESS.					
1. REPORT DATE (DD-MM-YYYY) 05-10-2013		2. REPORT TYPE		3. DATES COVERED (From - To)	
4. TITLE AND SUBTITLE An Evaluation of the Corrosion and Mechanical Performance of Interstitially Surface Hardened Stainless Steel				5a. CONTRACT NUMBER	
				5b. GRANT NUMBER	
				5c. PROGRAM ELEMENT NUMBER	
6. AUTHOR(S) Jones, Jennifer Lynn				5d. PROJECT NUMBER	
				5e. TASK NUMBER	
				5f. WORK UNIT NUMBER	
7. PERFORMING ORGANIZATION NAME(S) AND ADDRESS(ES)				8. PERFORMING ORGANIZATION REPORT NUMBER	
9. SPONSORING / MONITORING AGENCY NAME(S) AND ADDRESS(ES) U.S. Naval Academy Annapolis, MD 21402				10. SPONSOR/MONITOR'S ACRONYM(S)	
				11. SPONSOR/MONITOR'S REPORT NUMBER(S) Trident Scholar Report no. 416 (2013)	
12. DISTRIBUTION / AVAILABILITY STATEMENT This document has been approved for public release; its distribution is UNLIMITED.					
13. SUPPLEMENTARY NOTES					
14. ABSTRACT A surface hardening technique called "interstitial hardening" has been developed to introduce interstitial carbon atoms into stainless steel surfaces without the formation of carbides. Surface hardening of machine elements such as impellers or fasteners would improve performance regarding cavitation and galling resistance, and has intensified interest in this process. However, there remains a need to characterize and validate the specific performance characteristics of the hardened materials. In particular, the process parameters for which the corrosion resistance of the stainless steel is retained, rather than degraded, is of particular interest for marine applications. This project incorporated experimental testing conducted on 316L stainless steel that has been surface hardened using available commercial techniques, using both carbon and nitrogen as the interstitial atom. The hardness and thickness of the surface hardened layer is characterized and compared using metallography and microhardness profiling. The corrosion performance of the hardened surface is assessed using electrochemical potentiodynamic testing to determine the pitting potential in 3.5 wt. % NaCl solution. Corrosion fatigue and slow strain rate testing of untreated, hardened and damaged, hardened surfaces exposed to ASTM seawater is conducted. Finally, critical galling stresses are determined and compared. Post-test examination of damage attempts to identify mechanisms of material failure and characterize how corrosion-assisted cracks initiate and grow in surface-hardened materials.					
15. SUBJECT TERMS stainless steel, corrosion, fatigue, galling, hardening, fracture					
16. SECURITY CLASSIFICATION OF:			17. LIMITATION OF ABSTRACT	18. NUMBER OF PAGES 42	19a. NAME OF RESPONSIBLE PERSON
a. REPORT	b. ABSTRACT	c. THIS PAGE			19b. TELEPHONE NUMBER (include area code)

U.S.N.A. --- Trident Scholar project report; no. 416 (2013)

**AN EVALUATION OF THE CORROSION AND MECHANICAL PERFORMANCE OF
INTERSTITIALLY SURFACE HARDENED STAINLESS STEEL**

by

Midshipman 1/c Jennifer L. Jones
United States Naval Academy
Annapolis, Maryland

Certification of Advisers Approval

Associate Professor Michelle G. Koul
Mechanical Engineering Department

Associate Professor Joel J. Schubbe
Mechanical Engineering Department

Acceptance for the Trident Scholar Committee

Professor Maria J. Schroeder
Associate Director of Midshipman Research

Abstract:

A surface hardening technique called “interstitial hardening” has been developed to introduce interstitial carbon atoms into stainless steel surfaces without the formation of carbides. Surface hardening of machine elements such as impellers or fasteners would improve performance regarding cavitation and galling resistance, and has intensified interest in this process.

The interstitial hardening technique involves an activation step where the protective oxide film is removed from the surface in order to allow appreciable diffusion of the interstitial atom into the material at temperatures below which precipitate phases will form. Commercial processes have been developed to do this using halogen gases or plasma. However, there remains a need to characterize and validate the specific performance characteristics of the hardened materials. The stability of the hardened surface and the reproducibility of the process on various substrates need to be verified. In particular, the process parameters for which the corrosion resistance of the stainless steel is retained, rather than degraded, is of particular interest for marine applications.

This project incorporated experimental testing conducted on 316L stainless steel that has been surface hardened using available commercial techniques, using both carbon and nitrogen as the interstitial atom. The hardness and thickness of the surface hardened layer is characterized and compared using metallography and microhardness profiling. The corrosion performance of the hardened surface is assessed using electrochemical potentiodynamic testing to determine the pitting potential in 3.5 wt. % NaCl solution. Corrosion fatigue and slow strain rate testing of untreated, hardened and damaged, hardened surfaces exposed to ASTM seawater is conducted. Finally, critical galling stresses are determined and compared. Post-test examination of damage attempts to identify mechanisms of material failure and characterize how corrosion-assisted cracks initiate and grow in surface-hardened materials.

KEYWORDS: stainless steel, corrosion, fatigue, galling, hardening, fracture

Acknowledgments:

Center for Corrosion Science and Engineering, Code 6134, Naval Research Laboratory
Metallurgy and Fasteners Branch, Naval Surface Warfare Center, Carderock Division

Table of Contents

1. Introduction and Background	3
2. Experimental Methods	7
3. Results and Discussion	17
4. Conclusions	29
5. Future Work	30
6. References	31
7. Appendix	32

1. Introduction/Background

Ship designers and the Navy, in general, are continually looking for stronger and harder alloys to improve the performance and lifetime of structures and platforms. Engineers are looking for high strength materials to improve performance and safety, while maintaining low weight requirements. Strength limitations have directly affected marine applications in regards to material selection; particularly the tradeoff between ductility and strength. Engineers are actively looking for alloys with bulk material properties sufficient for manufacturing and use, while providing corrosion resistance and maintaining or improving mechanical properties.

For example, the Navy is currently facing alloy selection difficulties with some of their new platforms. Two specific issues found in marine applications are the cavitation of impellers and the galling of fasteners. The impellers of ships are susceptible to cavitation damage, which is a term describing the damage that arises from the implosion of bubbles that form at the material surface due to extreme cyclic pressure variations.¹ The implosion of these bubbles wears away the material over time, causing the need for frequent replacement.

A second example where stronger materials would be desirable has to do with a phenomenon called galling. Galling occurs when two materials are fastened together and become “cold-welded” or stuck together. Subsequent attempts at fastener removal will often shear the material, resulting in the need for a complete replacement. The shearing of bolt heads or threads are the results of the welded conditions created by the galling materials. Repairs are nearly impossible and replacements are expensive and difficult to install.² Corrosion resistant materials such as aluminum, titanium and stainless steels are particularly susceptible to galling.

These two issues can be remedied by using harder or stronger materials. However, components made from stronger materials are often less resistant to cracking under dynamic loading, less

corrosion resistant, and more costly. A solution to this problem is targeting weaker areas in the structure of the material. Hardening the surface of the component helps to retain the ductility of the component, while still providing the strength where it is needed. One can strengthen or make a material more wear-resistant through the process of adding carbon atoms to a metal's microstructure at the surface, known as "carburization."³ While a popular method, the carburization of chromium-containing alloys, such as stainless steel, results in the production of chromium carbides that degrade corrosion resistance. This degradation has resulted in the limitation and exclusion of surface hardened stainless steels from use in corrosive environments.

A new carburization technique, entitled interstitial hardening (IH) at low temperatures, has been designed to introduce carbon into stainless steel surfaces, while suppressing the formation of carbides.² The IH process focuses on inserting carbon atoms into the spaces between the iron atoms in the stainless steel microstructure as illustrated in Figure 1. This technique builds on the theory that the atomic motion, or diffusion, of substitutional atoms (chromium or nickel) is slower than the diffusion of interstitial atoms (carbon).² The process is conducted under low temperatures rendering the larger atoms stationary, but allowing the diffusion of carbon into the subsurface of the steel. The presence of carbon atoms helps to reduce the movement of iron atoms, which helps to increase the overall strength of the metal. The surface hardness, or strength, increases as more carbon is introduced into the microstructure.

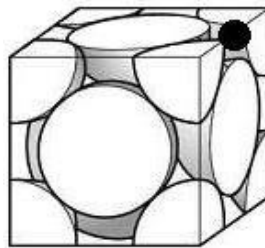


Figure 1 – Carbon interstitial atom (black sphere) in an interstitial site in face-centered cubic structure consisting of Fe atoms (white spheres).⁴

Carburization is traditionally carried out at high temperatures to maximize the ability of the carbon to diffuse throughout the surface. Upon cooling with the standard procedure, a large percentage of the chromium atoms from the stainless steel are removed from the surrounding material to form the chromium carbides. Since the chromium is responsible for producing a protective oxide film on the stainless steel, the reduced chromium content degrades the corrosion resistance and the steel is no longer “stainless.”

The time-temperature-transformation (TTT) diagram in Figure 2 shows three possible paths for the carburization of austenitic stainless steel.⁴

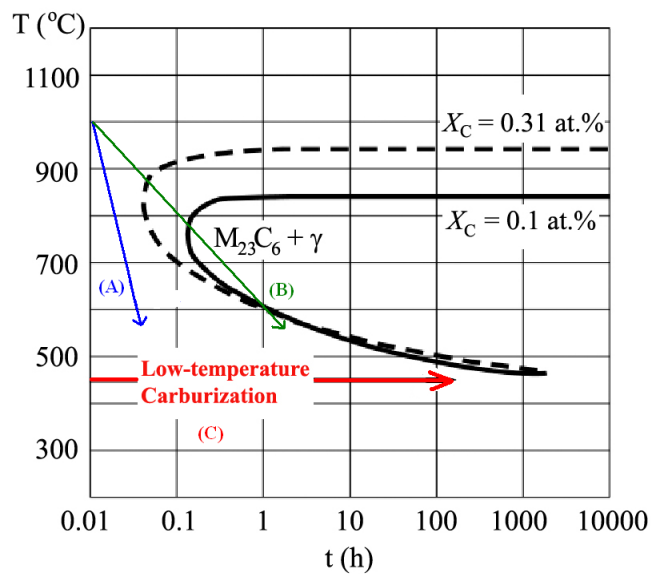


Figure 2: Time temperature transformation (TTT) diagram of carbide formation in stainless steels

(M is typically chromium).⁴

Path A shows an extremely steep cooling rate, which avoids the formation of carbides, but is difficult and expensive for large-scale productions. Path B models a moderate cooling rate which is typical of industrial processes, but as the cooling rate passes through the ‘nose’ of the “C” curve, carbides begin to precipitate out. Path C is a representation of the IH cooling process. By treating

the metal at a constant low temperature, the diffusion of chromium atoms is greatly reduced. Path C completely avoids intersecting the “C” curve on the TTT diagram (Figure 2).⁴ The carbon enters the material and remains an interstitial atom dissolved in the face-centered cubic structure of the steel (Figure 1)⁵, which results in different chemical and mechanical properties compared to the carbide ($M_{23}C_6$) particle that forms during Path B. Corrosion resistance is not immediately degraded due to the fact that the chromium content is not altered. In fact, carbon by itself is an inert and corrosion-resistant material and initial testing indicates that this surface can actually be more corrosion resistant than the original steel.³

These carburization methods hold great promise and interstitial hardening has been called “a new branch of materials science.” However, there remains a need to characterize and validate the beneficial effect of the surface hardening process on performance, and to ensure this surface hardening technique does not result in unforeseen degradation in other properties of the material. In addition, there is a desire to optimize the processing parameters to enable the treatment of large parts, and eliminate some of the more hazardous and expensive treatment steps. If IH treatments are proven to be durable under material testing, the Navy’s selection of these treated alloys would dramatically increase. The service life of components would be extended, thus increasing the readiness of naval forces, as well as reducing total life cycle costs.²

2. Experimental Methods

Material Properties:

316L Stainless Steel was selected to undergo the interstitially hardening process on the basis of its relatively simple microstructure.³ The percent composition of the untreated 316L Stainless Steel can be found in Table 1 and the corresponding typical material properties in Table 2.

Element	C	Mn	Si	P	S	Cr	Mo	Ni	N
Max % Composition	0.03	2.00	0.750	0.045	0.030	18.00	3.00	14.0	0.10

Table 1: Maximum Percent Composition of Elements in 316L Stainless Steel⁶

UTS ksi (MPa)	0.2% YS ksi (MPa)	% Elongation at Failure	Rockwell Hardness B
88.9 (613.1)	64.3 (443.3)	56.7	92.7

Table 2: Typical Mechanical Properties of 316L Stainless Steel

Interstitial Hardening of Specimens:

The Naval Research Laboratory (NRL) provided specimens after consultation with the United States Naval Academy. The surface hardening processes and initial metallurgical characterization were performed as part of the ongoing research program with the Naval Research Laboratory. A summer internship at NRL provided an opportunity for the initial testing to be conducted. BodyCote, the company heat-treating the interstitially hardened samples, treats the samples between 880°C and 980°C and diffuses carbon into the microstructure at the surface.⁷ The hardening process is completed in three steps: a thermochemical process in a furnace to enrich the surface in carbon, quenching in an oil or water solution, and a tempering operation varying in time and temperature dependent on the required application of the metal.⁷

Evaluation of Pitting Corrosion Susceptibility:

Corrosion is the destructive result of electrochemical reactions between a metal and its environment. A common form of corrosion in stainless steel is called pitting. Pitting is a localized form of corrosion in which small holes form on the top of the surface and move vertically into the material.⁵ Stainless steel is extremely susceptible to pitting corrosion in seawater and this type of corrosion often goes undetected by the naked eye until failure.

Potentiodynamic Polarization testing was conducted to determine localized corrosion susceptibility. A current was supplied to the material to increase the driving force for corrosion by increasing the electrochemical potential, or voltage, at a constant rate in the positive direction (Figure 3). The initiation to pitting corrosion is indicated at the point where the current density (i), current per unit of sample area, rapidly increases with little voltage change (arrow, Figure 3).⁸ A more positive potential for the initiation of pitting corrosion indicates the need for a higher driving force to initiate corrosion, and correlates with a smaller likelihood that pitting corrosion will occur under service conditions.⁵ Figure 3 shows an example polarization curve for an untreated stainless steel sample. As shown in the figure, pitting will have difficulty initiating or propagating at potentials less than 300 mV due to the passive layer. This passive layer helps to prevent pitting corrosion and is present in stainless steels due to the chromium concentration in the microstructure. As the potential increases, the passive layer can reform and adapt when damaged to protect the surface from corrosion. After the pitting potential is exceeded, the passive layer is damaged and cannot reform.¹³ A successfully treated sample would be able to reach a higher breakdown potential than the noncarburized sample.

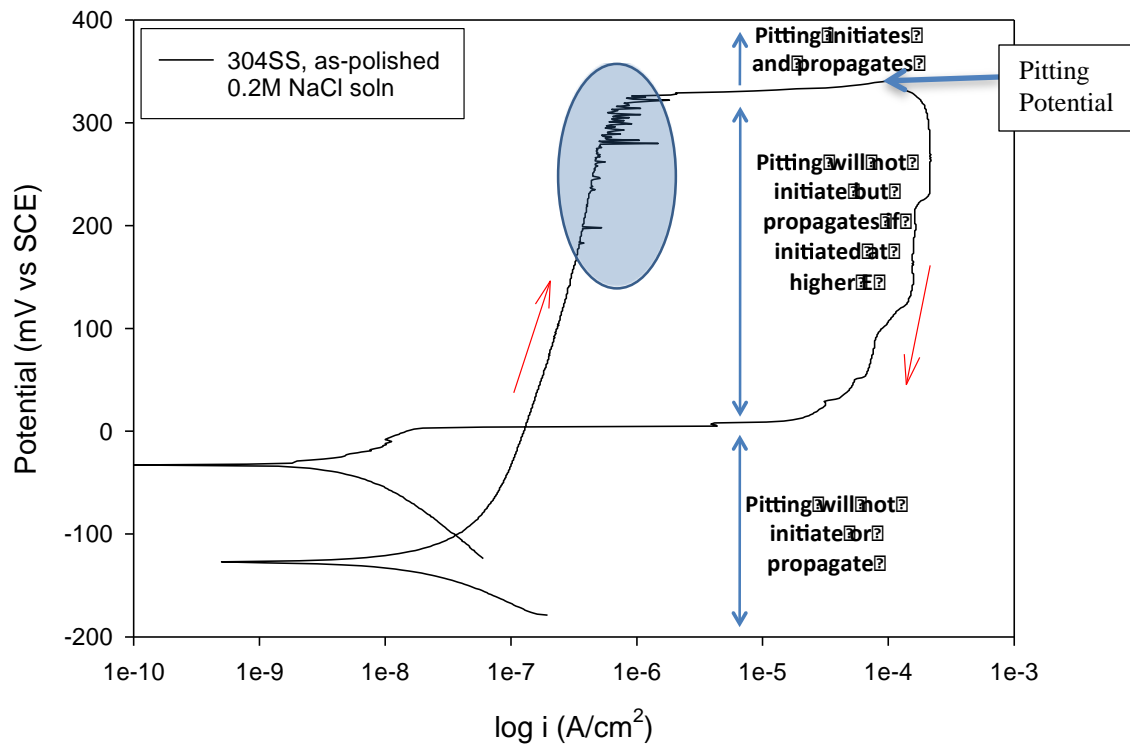


Figure 3: Representative potentiodynamic polarization curves showing pitting resistance evaluation⁸

Similar experiments were conducted on treated and untreated stainless steel to assess the effect of the IH process. The polarization testing procedure involved using a flat cell compressing the sample to a backing plate. A rectangle with area less than 100 mm² was isolated by electrical tape and exposed to seawater. The samples were polished with 600 grit sandpaper and tested in 3.5 wt% seawater. An open-circuit potential was established for 12 hours, followed by a period of anodic polarization with a scan rate of 0.1667 mV/sec. The scan was programmed to reverse direction at a critical potential of 1.5 V or current density of 1 mA/cm², whichever came first. The measured current was divided by the area of the sample to report current density.

Fatigue performance was measured by conducting fatigue testing under fully reversed bending measured in air and under an artificial seawater drip where the surface was continuously wetted. Surface hardened specimens (Figure 4) were mounted, aligned with strain gages, and then cycled through alternating reverse bending loads until failure. At least three different stresses were tested to obtain the transition between a finite and infinite fatigue life observed in an S-N Curve. If the sample life exceeded 10^7 cycles, the test was stopped and considered a “run-out.” Samples tested in air were tested at a 32 Hz frequency and samples in seawater were tested at a slower frequency of 16 Hz in order to allow for more corrosion damage to accumulate. Results of the treated samples were compared to the S-N curve of the untreated samples in air and in seawater to detect any changes.⁹

Figure 5 shows the fatigue testing apparatus setup for seawater testing. Fatigue initiation is coincident with failure, which allows the apparatus to be deflection controlled rather than load controlled. Deflection is set by applying the desired testing load, measuring the deflection, removing the load, and setting the eccentricity scale to the corresponding deflection.

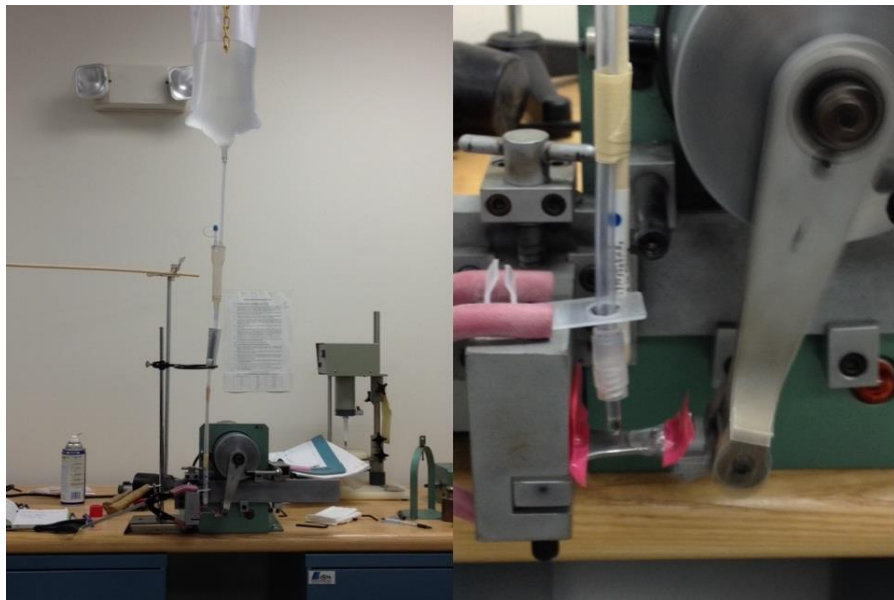


Figure 5: Fatigue Testing Apparatus for Samples in Seawater

The applied load is converted to stress values via cantilever beam calculations assuming elastic behavior for the specimen's shape. The specimen geometry is purposefully designed that a change in the moment of area (I) is compensated by the change in moment along the long axis of the specimen, resulting in a constant stress for the gage width (Figure 4). Stress is calculated from the load via the following equation, where a is the distance between the left edge and a point on the sample, P is the applied load, b is the width, and h is the height or thickness of the sample.¹⁰

$$(1) \quad \sigma = \frac{-6aP}{bh^2}$$

Evaluation of Environmentally Assisted Cracking Performance:

Environmentally assisted cracking (EAC) is the cracking of a material that occurs at unexpectedly low loads due to the combined effects of stress and the surrounding environment.¹¹ Stronger or harder materials are typically more susceptible to EAC. There are different forms of EAC: stress corrosion cracking (SCC), corrosion fatigue (discussed in previous section) and hydrogen-assisted cracking (HAC).¹² To evaluate SCC and HAC resistance, a slow strain rate test is utilized. A slow dynamically increasing strain is externally applied on a sample for evaluation. The slow extension of the sample results in a slow but constant strain rate in the range from 10^{-4} to 10^{-7} in/s, and allows time for the corrosion process to have a deleterious effect on cracking and measured ductility.¹¹ The slow strain rate test is used for comparative evaluation of differing environmental and metallurgical variables. Typically, results from the tests conducted in the test environment correlate to performance in service.¹¹

The tensile specimens in this study were tested at a slow strain rate of 9×10^{-7} in/s. Test cells were utilized to submerge the sample in a seawater environment and seawater with a cathodic protection. For the samples that experienced cathodic protection, a constant cathodic or negative voltage of -1.0 V vs. the SCE (saturated calomel) reference electrode was applied to the sample by

supplying the appropriate current to maintain this potential. This current supplies electrons to the steel, making it the cathode in an electrochemical cell, similar to an impressed current cathodic protection system and protects it from corrosion.¹³ A byproduct of cathodic protection, however, can be the generation of hydrogen gas at the protected material's surface. If a significant portion of the hydrogen enters the material rather than forming gas, it can cause embrittlement and HAC. Therefore, this process helps to protect the sample from corrosion, but can promote hydrogen embrittlement.¹³ Stronger materials are often more susceptible to HAC, therefore the susceptibility of the hardened surface to this form of embrittlement is investigated.

The resulting data sets are used to calculate stress as a function of percent elongation. Stress vs. Percent elongation graphs for the different testing conditions will yield comparable results for the ultimate strength and elongation at failure for each sample. The percent reduction in area (%RA) will be calculated from the fracture area measured from photographs (A_f) via the equation below:

$$(2) \quad \%RA = 100 \frac{A_o - A_f}{A_o}$$

where A_o is the original cross section of the specimen gage.

Both the percent elongation at failure and %RA are measures of the ductility of the sample, and will be reduced in instances where SCC or HAC have taken place. Testing will be supplemented by a microscopic examination of the fracture surface.

Carbon by itself is an inert, corrosion resistant material. The addition of interstitial carbon to the microstructure can render the surface of the material more corrosion resistant than the interior of the material. If a scratch or crack were present, the corrosion resistant surface and the less corrosion resistant interior would be in electrical contact and exposed to the corrosive environment. This arrangement is effectively an electrochemical battery, also called a "galvanic couple," where

the less corrosion resistant material will become the anode and corrode more severely by being part of this galvanic couple (Figure 6).¹³ The large surface area of the corrosion resistant material will drive the corrosion of the exposed interior metal, perhaps causing damage over time. Slow Strain Rate Testing (SSRT) of specimens with intentional defects that expose the interior metal were tested for increased susceptibility due to this galvanic interaction. Specimens with 100 micron deep circumferential notches, created with a thread cutting tool, were machined to expose the base metal during SSRT tests conducted in air and seawater, similar to what is shown in Figure 6.

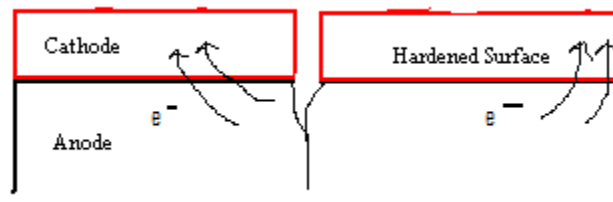


Figure 6 – Example of possible Galvanic Corrosion of base metal with a nobler, hardened surface.

Evaluation of Galling Resistance:

Galling is most prevalent with fasteners made of stainless steel and other alloys which possess a naturally forming oxide surface film that provides corrosion resistance. During tightening, the build-up of pressure causes the oxide film to break and the bare metal interfaces bond. Galling can also be referred to as “cold-welding,” and results in the materials becoming “stuck” together.³ Galling is a result of exceeding a threshold pressure. Surface damage occurs when the mating materials are moved relative to each other and the cold-welded, or galled, areas of the materials are sheared apart. A predisposition towards galling can lead to increased tendencies towards cracking, breakage, or stripped threads in fastener applications. Once galling has occurred, repair is nearly impossible, resulting in a need for a completely new component.³

ASTM (American Society for Testing and Materials) has standard methods (Designation G98-02)¹⁴ of testing galling resistance though measuring the threshold galling stress. A galling rig

was designed to hold the cylindrical test samples. A compressive testing frame was used to maintain a constant, compressive load between two flat specimens. One specimen is slowly rotated manually by a wrench, while the other remains stationary (Figure 7). The surfaces are examined for galling after every load increase and 360-degree rotation. The threshold galling stress is the stress midway between the highest non-galled stress and the lowest galled stress.¹⁴ This test method can rank materials in their resistance to failure by galling. Interstitially hardened specimens (highlighted in blue in Figure 7) will be compared to untreated specimens to evaluate the effect of the IH process on galling resistance.

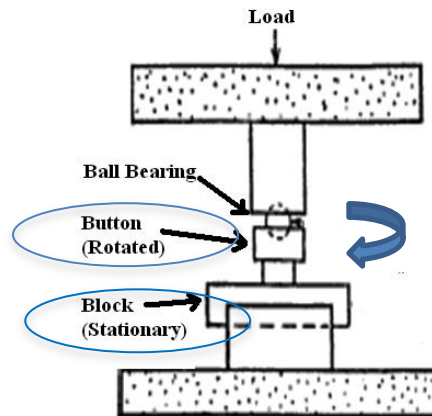


Figure 7: Galling Test Set-Up. Circled Parts Consist of Untreated or Treated 316L Stainless Steel¹⁴

Post-Test Examination:

Scanning electron microscopy is a valuable tool to metallurgists to determine possible causes of material failure. Fatigue, EAC, galling and corrosion specimens are examined with both optical and electron microscopy to attempt to identify the mechanisms associated with cracking and corrosion suppression and/or failure. Figure 8 is an example of how optical microscopy can be used to examine the crack path in a material.

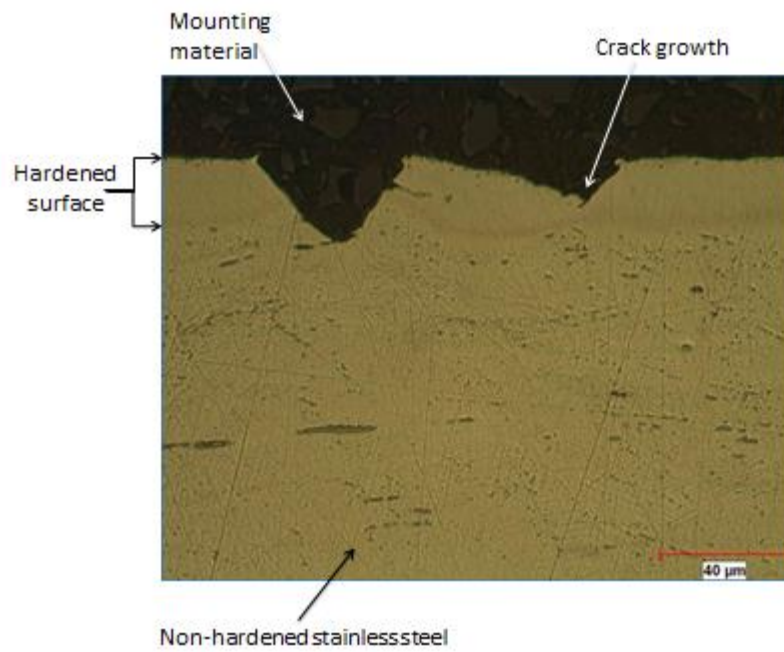


Figure 8 – Side view of B1Process hardened SSRT specimen after testing in seawater.

3. Results and Discussion

Evaluation of Pitting Corrosion Susceptibility:

Corrosion testing was used for an initial screening of properties between untreated stainless steel and three commercially available treatment processes. Processes A-C utilized different activation steps and treatment processes to hardened the 316L stainless steel samples. Figure 9 shows the polarization curves for the four samples.

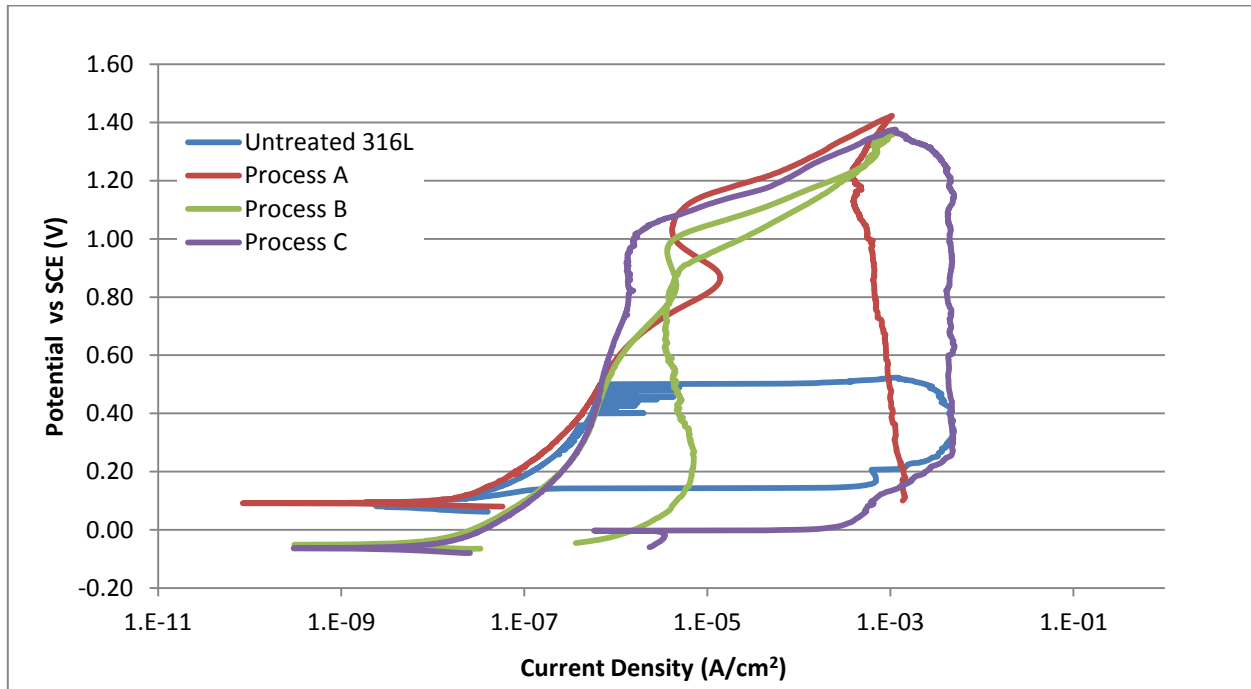


Figure 9: Potentiodynamic polarization curve for untreated stainless steel and three treatment processes

The initiation for pitting corrosion for the untreated stainless steel is approximately 0.50 V, whereas the treated samples reach a much higher voltage before plateauing and re-passivizing during the test. Overall, the treated samples were able to reach much higher voltages (indicated by red, green, and purple lines) than the untreated sample (blue line), showing that the process of interstitially hardening maintains and helps to improve corrosion resistance. This graph shows that the different commercial hardening processes were successful in treatment, because they had a higher breakdown potential before plateauing than the untreated samples. Processes A, B, and C were treated by

different companies, resulting in variability among the activation methods, carburizing treatment temperature and length. These differences can be seen in the reverse scans of the polarization curves in Figure 9. Process B was selected for further testing, based on its ability to re-passivate upon the scan reversal and follow a similar return path indicating that the passive layer did not sustain any damage. Process A and C did not re-passivate, indicating a larger amount of corrosion damage during the forward scan, similar to the graph in Figure 3. These graphs and other variability in the slow strain rate data show the effect that production parameters play in the mechanical behavior of the material. After selecting Process B to focus on, further research was conducted in the areas of fatigue resistance, environmental cracking resistance, and galling performance.

Metallurgical Evaluation:

Microhardness testing was conducted for Processes B1 and B2, which represent treatment from the same commercial company, but slightly different hardening process batches. These samples were treated with the same hardening process, but for slightly different temperatures and times, which can have slight variations on the overall mechanical properties. Different temperatures and times affect the penetration of carbon into the surface and properties can vary depending on carbon depth. SSRT (bar), fatigue and corrosion samples (sheet) were hardened using the processing parameters designated B1. SSRT (bar) and galling samples (sheet) B2 from a different heat of stainless steel were hardened using slightly different processing parameters and designated B2. The Vicker's microhardness of the fatigue samples were measured as a function of depth perpendicular to the sheet face as well as perpendicular to the sheet edge. The microhardness of the SSRT samples was measured as a function of depth perpendicular to the surface, in the radial direction of the bar. The hardened surface layer is resistant to etching, so by measuring the depths of

the unetched regions, the depth of penetration of carbon into the sample could be measured (Figure 10).

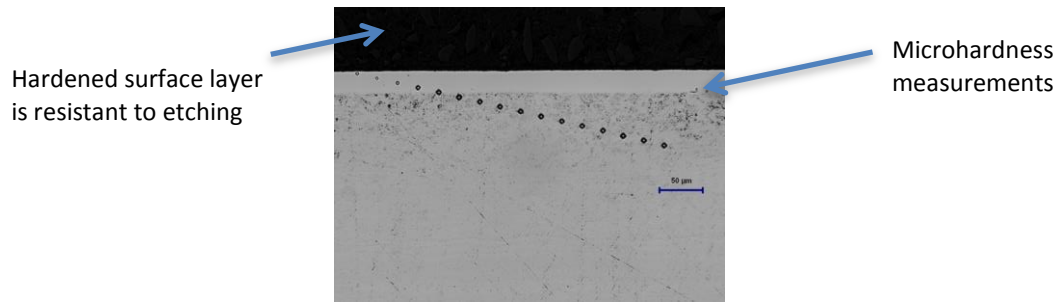


Figure 10: Etched profile of a hardened sample

Figures 11a and 11b show the hardness measurements as a function of depth from the surface for two different batches of Process B. The vertical lines on the graphs illustrate the measured depth of the hardened surface layer. For B1, the fatigue sheet faces had a measured depth of 26 microns and a depth of 29 microns for the edges. The slow strain rate bar samples had a measured depth of 22 microns. For B2, the fatigue sheet faces had a measured depth of 33.9 microns and a depth of 36 microns for the edges. The slow strain rate bar samples had a measured depth of 40.9 microns. Even with the differing carbon depths (Figure 11), the increase in hardness at the surface was around three times that of the interior for all the samples.

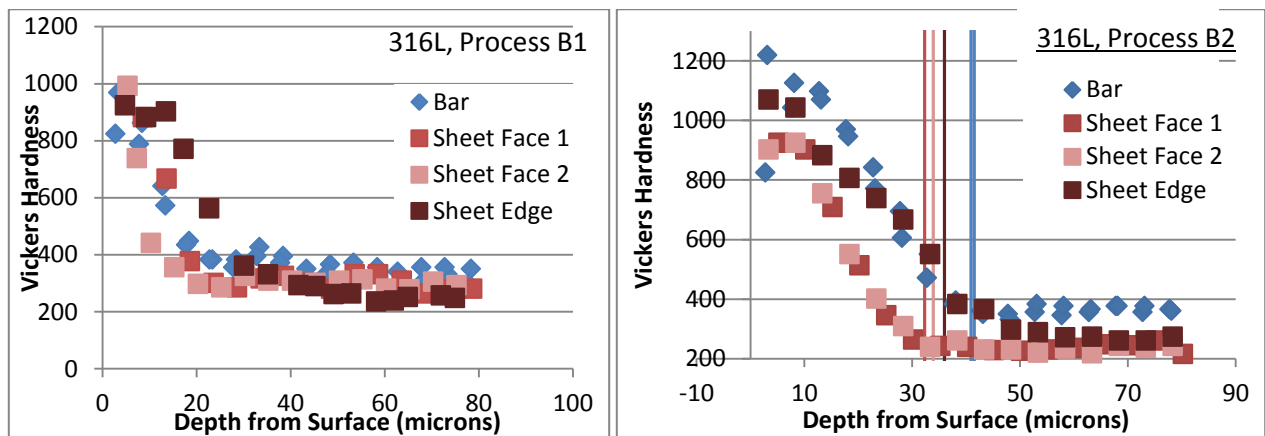


Figure 11: Hardness as a function of depth into the material for (a) Process B1 and (b) Process B2

Evaluation of High Cycle Fatigue and Corrosion Fatigue Performance:

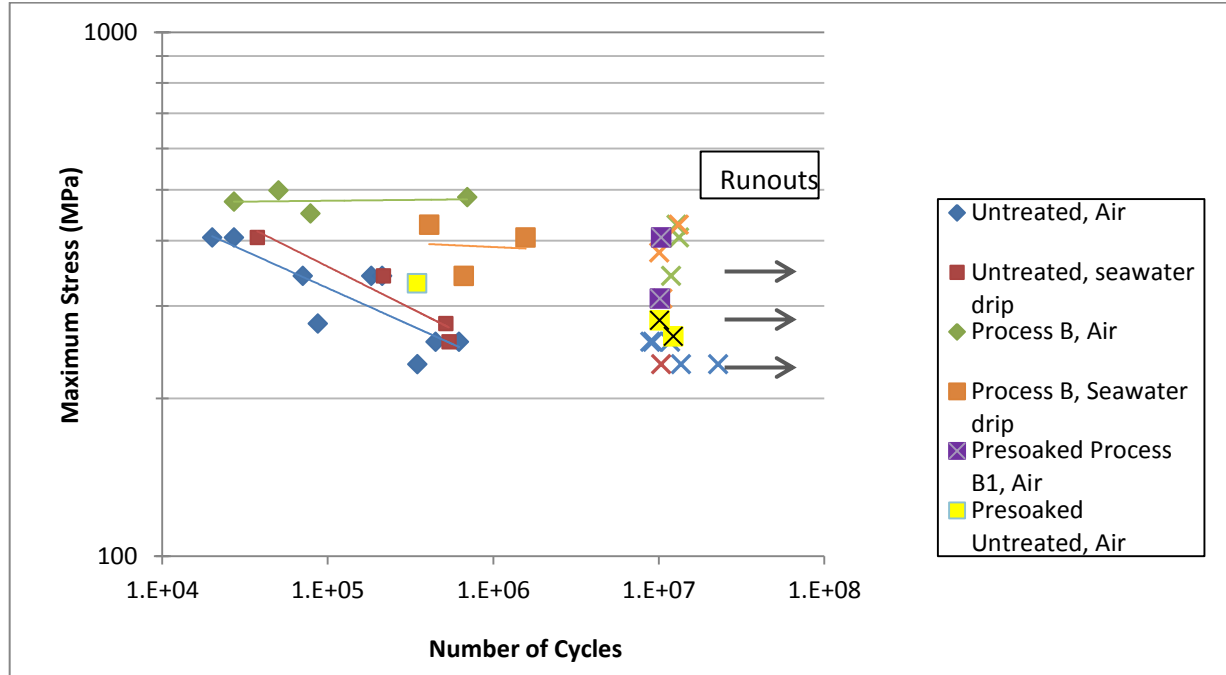


Figure 12: S-N curve for untreated and treated 316L stainless steel in air and seawater

Figure 12 shows the fatigue behavior for untreated and treated 316L stainless steel in air and seawater. In addition, five samples (two treated, three untreated) were presoaked in seawater for three months to presumably accumulate corrosion damage before being tested in air. A lifetime greater than 10,000,000 was considered a run-out and subsequently stopped. Data points that are marked as “X” points and have arrows close to them are considered “run-outs,” meaning that the sample did not break for the duration of the test. The untreated data served as a baseline to validate the fatigue machine accuracy and serve as a comparison to the treated samples. The fatigue limit of steel is typically 35-60% of the tensile strength of the steel, which agrees with the obtained results.⁵

Increasing the surface hardness helps to suppress crack initiation and increase fatigue life. At an applied stress of 400 MPa, surface hardening increased the fatigue life from approximately 30,000 cycles to more than 10 million cycles. Unlike the air tests where fracture initiates at the sheet face, the fractography of the hardened samples shows initiation at corners, visible beach

marks and brittle fracture at the surface at a smaller depth than the measured hardened surface layer. This fracture pattern could be indicative of a critical carbon content percentage where more brittle fracture occurs rather than ductile fracture (Figure 13). In bending, stress is at a maximum at the surface and decreases with depth, which also could be an effect when analyzing the fracture patterns.

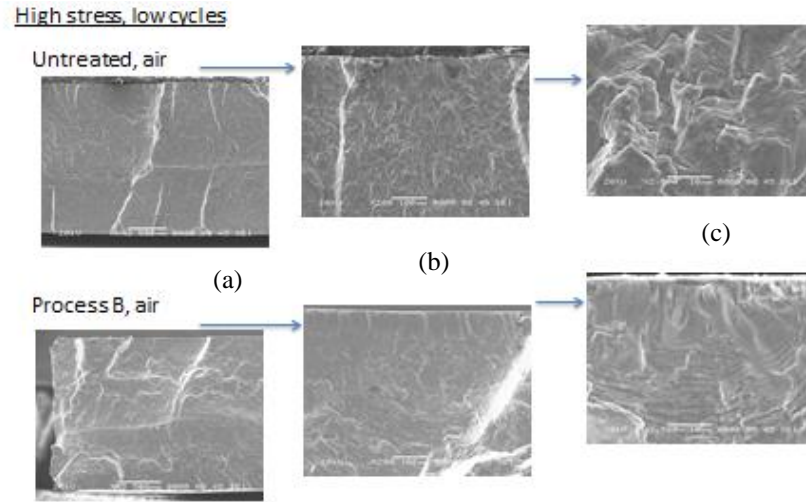


Figure 13: Scanning Electron Microscope (SEM) stress fracture images at (a) x43, (b) x200, (c) x2500 magnification for untreated and treated fatigue samples in air

All fatigue fracture surfaces were examined with the Scanning Electron Microscope (SEM). Figure 13 shows an untreated and treated sample tested under high stress in air, under increasing magnification moving left to right. When examining the treated samples, a brittle to ductile fracture area is seen when moving from the surface to the interior of the sample. This transition area is due to the hardened surface and the decreasing carbon content while moving vertically into the sample. Results confirm that sample crack initiation is seen from only one side at low stress and from both sides at high stress for the untreated and treated samples (Figure 14), which is typical fatigue behavior.¹⁵

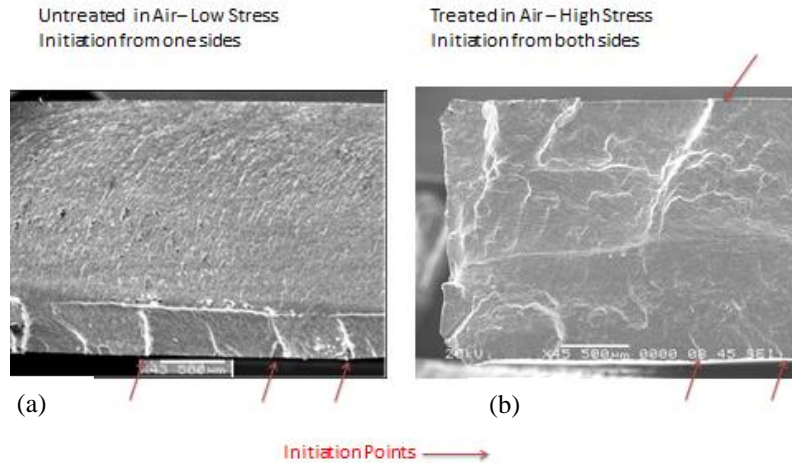


Figure 14: Initiation analysis of the fracture surface at (a) x43 low stress untreated and (b) x45 high stress treated fatigue samples in air

Upon further examination of the brittle fracture initiation zone in the treated samples, it appears that the initiation zone has moved subsurface with the hardened samples. Figure 15 shows a treated sample in air that exhibits brittle fracture confined to ~10 microns below the surface, but the carbon infused area was measured to 26 microns deep. It appears that there is a critical carbon content percentage for seeing brittle failure fracture patterns.

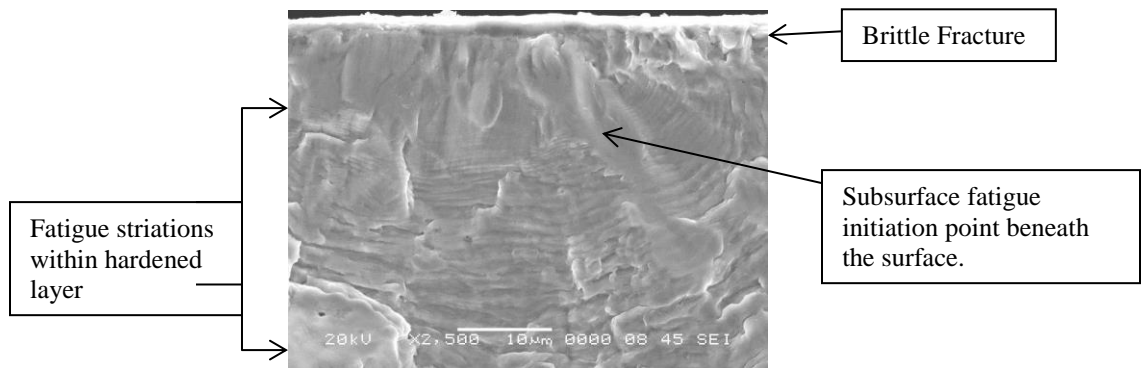


Figure 15: Brittle to ductile fracture area for a treated fatigue sample (x2500) in air

For the fatigue testing, seawater has a minimal effect at the frequencies employed; however, the scatter in the high cycle data appears to be more significant for seawater exposures of the surface hardened material. This scatter could be a result of the 16 Hz testing frequency not being slow enough to allow corrosion damage to occur. There was little to no difference in the life cycle

length between the samples presoaked in seawater and the samples tested with an active seawater drip (Figure 12). Further investigation into the duration of time soaked and the effect on fatigue life could be of interest. Figure 16 shows SEM scans of two samples that had similar life cycle lengths, but the seawater sample was tested at a load ~150 MPa less than the sample in air.

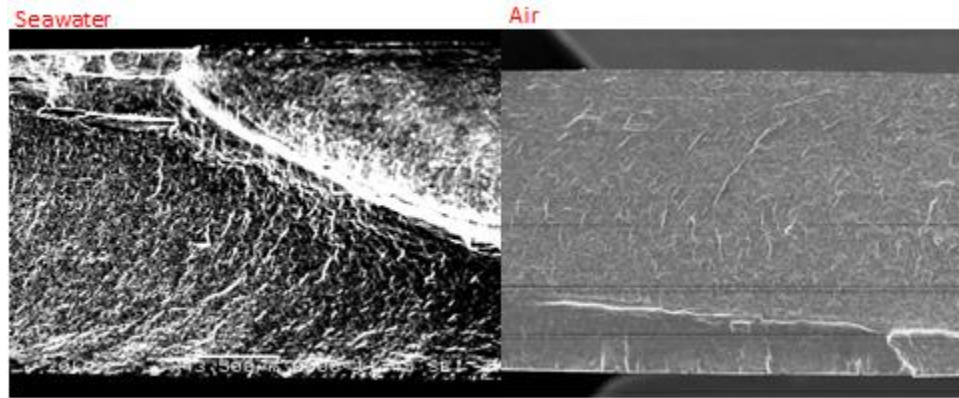


Figure 16: SEM stress fracture images (x43) for treated fatigue samples tested in seawater and air

The fracture surface of the hardened samples in seawater appear to have initiated at the corners (as in the air tests), and there are visible signs of rust associated with these assumed initiation sites, indicating that corrosion may have been playing a role (Figure 17).

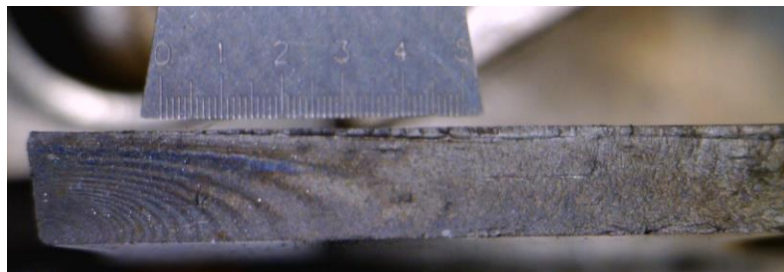


Figure 17: Optical image of the fracture surface for a treated fatigue sample tested in seawater

Evaluation of Environmentally Assisted Cracking Performance:

Fifteen samples were tested with the slow strain rate testing mechanism under varying conditions with a strain rate of 9×10^{-7} in/sec. Nine samples were from the B1 batch and six samples were from the B2 batch. Before treatment, one sample from the B1 batch and three from the B2 batch were

saved in their untreated form to be used later for baseline testing and comparison to the treated samples. Samples were tested in air, ASTM seawater, and with a cathodic protection in ASTM seawater. Two samples were pre-notched and tested in air and ASTM seawater. Figure 17 shows the plots of the Stress vs. Percent Elongation data for the select, varying conditions for the B1 process.

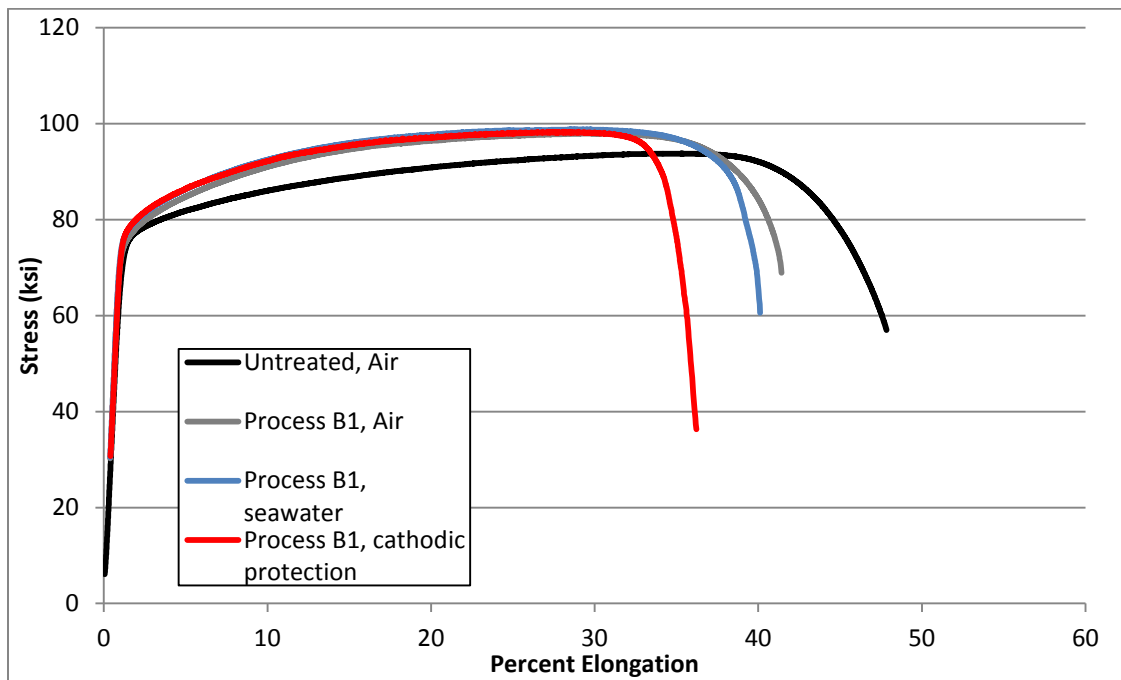


Figure 17: Slow Strain Rate Results for Process B1 in Air and Seawater

The hardened material sustained a higher stress before failure than the untreated sample in air, but experienced a 20% reduction in the percent elongation at failure. The effect of surface layer is like a notch toughening effect. The ultimate strength is increased and the ductility decreased due to constraint of interior material by the harder outer layer.¹⁷ This reduction in ductility could be a concern for applications using small hardened parts, but less of a concern for parts on a larger scale than examined by this study. The lower elongation at failure in the corrosive environment may indicate some susceptibility to EAC.

Two samples from the B2 process were pre-notched with a 60 degree V-notch before testing. Figure 18 shows the slow strain rate data of the pre-notched samples compared to smooth samples.

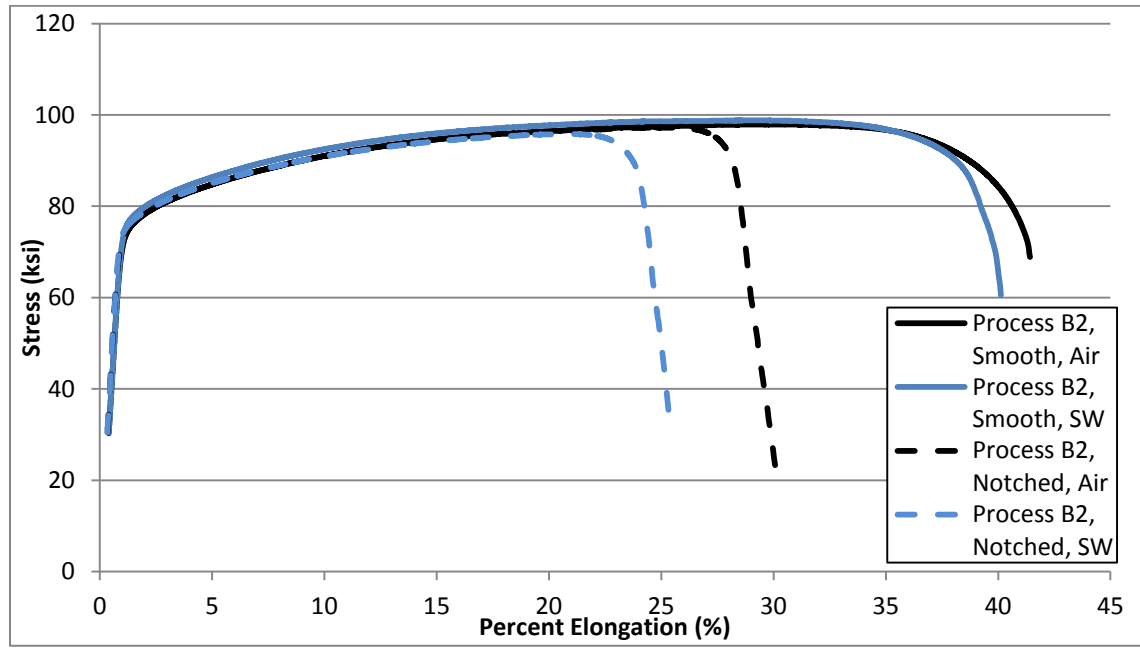


Figure 18: Slow Strain Rate Results for notched samples in air and seawater

As seen in Figure 18, seawater appears to have a larger effect on the failure of notched samples when compared to smooth. The percent elongation at failure was reduced as well as the ductility of the notched samples. These results warrant further examination on samples with larger exposed areas.

Independent of environmental effects, it is expected that the ductility will be lower with intrinsically stronger steel, which can result from heat to heat variations, or from the carburizing process. In order to examine the environmental effects independent of strength, the ductility data using percent reduction in area (Figure 19a) and percent elongation at fracture (Figure 19b) as a function of 0.2% yield strength are shown. The graphs show that seawater (the triangle blocks) appears to have little effect on ductility whereas cathodic protection (square boxes) seems to

consistently show the lowest values of ductility. However, the effect is small and not any larger for the hardened material compared to the untreated case (based on B2 process).

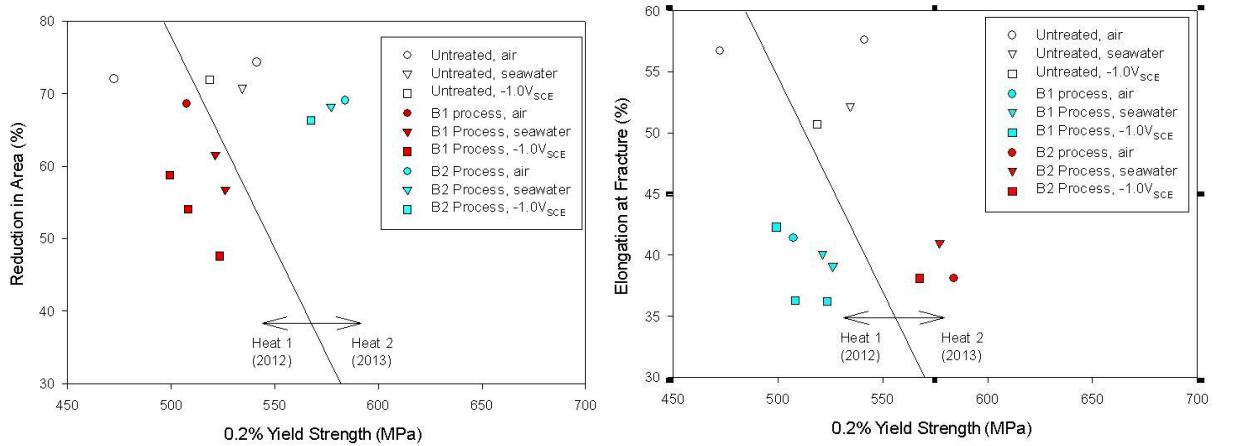


Figure 19a: Reduction in Area vs .2% Yield strength graph of the SSRT samples
b: Elongation at fracture vs .2% Yield strength graph of the SSRT samples

An analysis of the fracture surfaces of the SSRT data support the same conclusions (Figure 20).

Cathodic protection reduces the ductility of the surface hardened material to a small degree where larger secondary cracks were observed (Figure 20 c,d). Secondary cracking of the hardened surface was observed upon reaching the tensile strength (Figure 20 c,e). Brittle fracture was confined to a depth of 10 microns in the SSRT samples for samples tested in the different conditions.

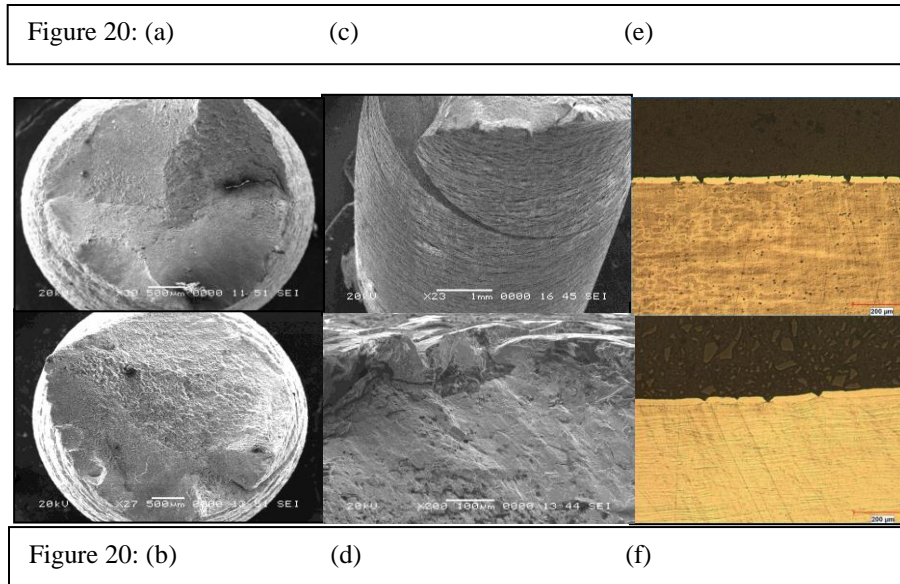


Figure 20: (a) 30x SEM capture of the untreated fracture surface in air
 (b) 27x SEM capture of the hardened material fracture surface in air.
 (c) 23x SEM capture of the hardened material fracture surface with cathodic protection.
 (d) 200x capture of the hardened surface with cathodic protection
 (e) Etched profile of the hardened surface with cathodic protection.
 (f) Etched profile of 316L showing a treated surface layer that underwent seawater SSRT testing

Evaluation of Galling Performance:

Due to sample availability, galling testing was only conducted on the B2 batch of hardened 316L stainless steel. Three conditions were tested on the B2 batch to assess galling resistance: an untreated button and square coupon, a combination – a hardened button and an untreated coupon, and a treated button and coupon. The image on the right in Figure 21 shows what would be considered galling damage. The damage is visible to the human eye and material loss can be identified. The picture on the left shows some superficial discoloration, but is not considered galling as the material remains intact after the test. The ring is a depression from the load, but no permanent damage occurred during testing.



Figure 21: Galling coupons post testing at different loads.
The sample on the left shows no trace of galling whereas the sample on the right galled.

Figure 22 shows the galling threshold for the three conditions. Results show that the treated process virtually eliminates galling as a concern, because the galling threshold is very close to the yield stress of the material. Hardening of only one of the mating surfaces nearly doubles the galling resistance as measured by this test.

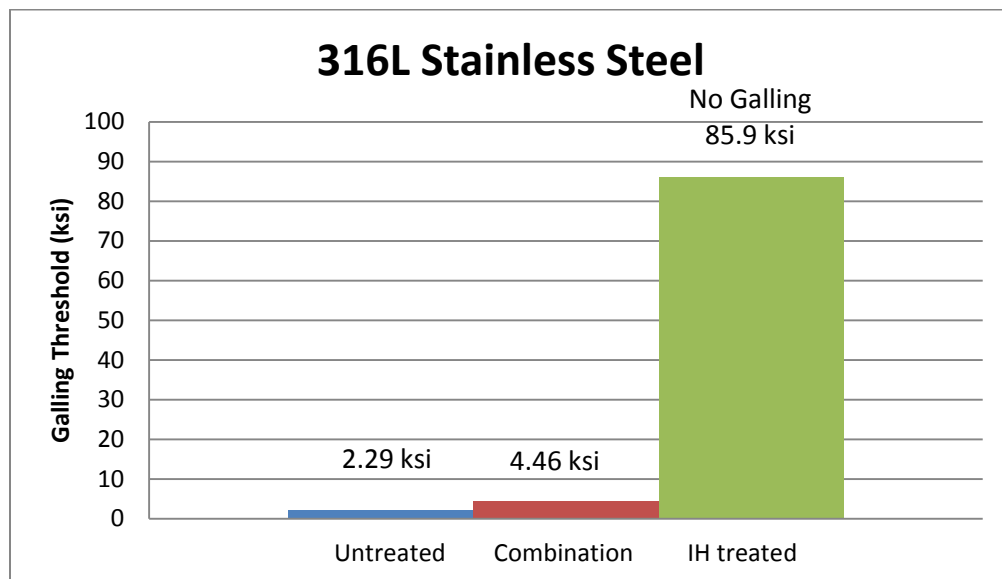


Figure 22: Galling tests on IH treated and untreated 316L stainless steel

4. Conclusions:

- The measured depth of the hardened surface agrees with the depth of the unetched region of the cross-sectioned specimens. In both the B1 and B2 processes microhardness indicates that carbon uptake may have been higher at the sheet edges than at the sheet faces. The difference in carbon uptake may be connected to the fatigue failure shifting to the corners of the samples.
- The IH hardening process “B” enhances the pitting corrosion resistance of 316L stainless steel as measured by a 500 mV increase in the breakdown potential.
- The surface hardened material shows a significant improvement in fatigue life compared to the untreated material in air. The endurance limit was increased from 256 MPa to 342 MPa due to the treatment process. Surface hardening appeared to shift the initiation site to the corners, where the surface was not as carefully prepared for hardening.
- A decreased lifetime, possibly due to seawater exposure, was noted for only one hardened specimen. Corrosion was visible at the corners of the hardened samples tested in seawater indicating a possible contribution of corrosion to cracking initiation.
- Brittle fracture at the outermost surface of the surface hardened fatigue specimens is noted, with striations beginning at a depth below the surface (10 microns), which was smaller than the depth of the hardened layer (25 microns).
- Surface hardened samples show higher tensile strength and lower ductility compared to untreated material when tested in air under slow strain rate conditions. The effect of seawater exposure and simulated cathodic protection do not drastically or consistently affect the ductility of the surface hardened material compared to identical tests in air.

- Surface fracture of a more brittle nature in the SSRT test is confined to a depth of 10 microns, which is less than the measured depth of carbon enrichment from microhardness and optical measurements.
- Seawater appears to have a larger effect on the failure of notched samples when compared to smooth.
- The galling stress for hardened surfaces approaches the yield stress of the material, virtually eliminating galling concerns. Hardening only one of the mating surfaces was found to nearly double the galling resistance from 2.29 ksi to 4.46 ksi.

5. Recommendations for Future Work Based on Results from this Study

- Investigate crack initiation and growth under conditions where the exposure of the untreated material is possible to expand upon the notched specimens tested in this study.
- Investigate how the size of the hardened part could play a factor into how much the hardening process will affect the ultimate strength and ductility.
- The increased scatter in fatigue seawater testing of the hardened material warrants further study and microscopic examination as to whether using a slower testing frequency or different exposure times to the environment would affect the results.
- The reduced ductility of the intentionally damaged IH specimen in seawater also indicates that further testing may be warranted to examine how great a defect in the surface layer would affect overall mechanical properties and component life expectancy.
- Investigate the hardness depths and profiles that develop as a function of product form and surface preparation to verify the repeatability and sensitivity of this IH

process to these conditions to see how great of an extent that varying treatment steps can affect overall mechanical properties.

Overall, the results from this study indicate that interstitial hardening holds promise for obtaining materials with exceptional wear and fatigue resistance, while also enhancing the corrosion performance of 316L stainless steel.

6. References

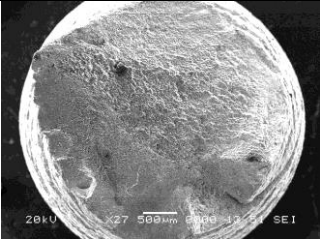
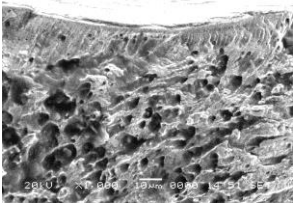
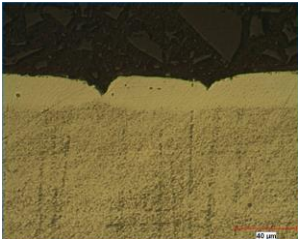
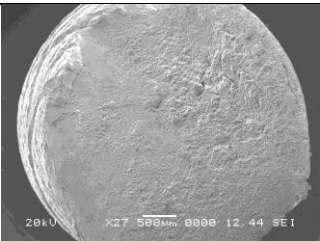
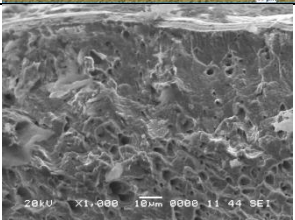
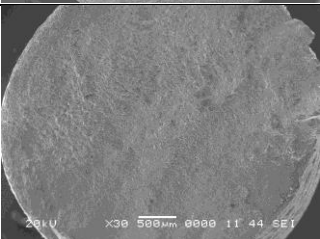
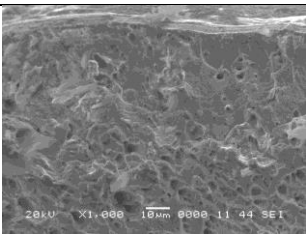
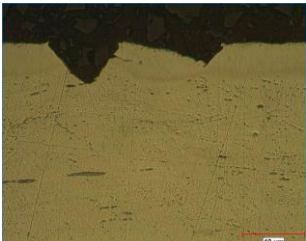
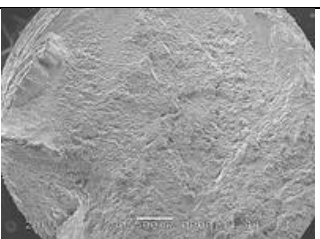
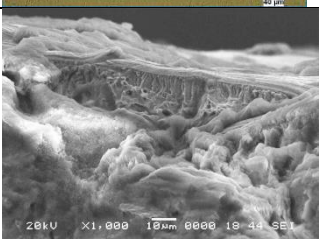
1. NRL Technical Strategy for Cavitation Resistant Alloys for Marine Propulsion Materials Presentation, 2007
2. Greenslade, Joe. "How to Stop Thread Galling on Stainless Fasteners." <http://www.estainlesssteel.com/gallingofstainless.html>
3. P.M. Natishan, F.J. Martin, E.J. Lemieux, T.M. Newbauer, R. Rayne, R.A. Bayles, "Carbon Surface Modification for Enhanced Corrosion Resistance", Chemistry Division, 2008 NRL Review.
4. P.C. Williams, S.R. Collins. "Mechanical Design using Low-Temperature Carburization", U.S. Department of Energy Field Report, (Dec 2008).
5. Rethwisch, D.G. and W. D. Callister Jr., *Fundamentals of Materials Science and Engineering: An Integrated Approach*, 3rd ed. (Wiley, John & Sons, 2007).
6. United Performance Metals. "316/316L Stainless Steel Sheet & Coil – Chemical." <http://www.upmet.com/products/stainless-steel/316316l/chemical>
7. "BodyCote: Atmospheric Carburising." <http://www.bodycote.com/en/services/heat-treatment/case-hardening-with-subsequent-hardening-operation/atmospheric-carburising.aspx>
8. Koul, Michelle. "Polarization Data from EM456," United States Naval Academy Mechanical Engineering Department, 2013.
9. NDT Resource Center. "S-N Fatigue Properties." <http://www.ndt-ed.org/EducationResources/CommunityCollege/Materials/Mechanical/S-NFatigue.htm>
10. Nisbett, J.K., and R. G. Budynas. *Shigley's Mechanical Engineering Design*, 9th ed. (McGraw-Hill Companies, 2010), 266.
11. "Standard Practice for Slow Strain Rate Testing to Evaluate the Susceptibility of Metallic Materials to Environmentally Assisted Cracking", American Society for Testing & Materials, 2000.
12. Craig, Benjamin and Richard Lane. "Environmentally-Assisted Cracking: Comparing the Influence of Hydrogen, Stress, and Corrosion on Cracking Mechanisms," *The AMPTIAC Quarterly* (2005). http://ammptiac.alionscience.com/pdf/AMPQ9_1ART02.pdf
13. McCafferty, E. *Introduction to Corrosion Science* (Springer, 2010), 342.
14. "Standard Test Method for Galling Resistance of Materials", American Society for Testing & Materials, Designation G98-02, 2009.
15. Sachs, Neville. "Understanding the Surface Features of Fatigue Fractures: How They Describe the Failure Cause and the Failure History," *Journal of Failure Analysis and Prevention* (April, 2005).
16. Hertzberg, Richard. *Deformation and Fracture Mechanics of Engineering Materials*, 3rd ed. (Wiley, 1989), 246.


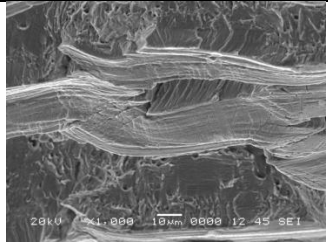

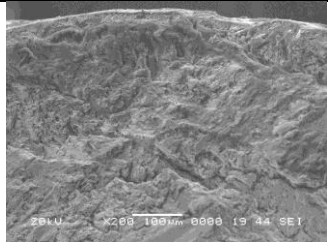
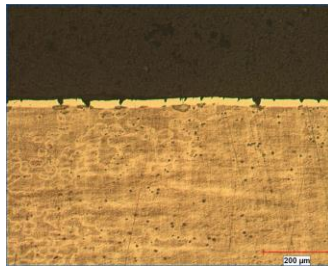
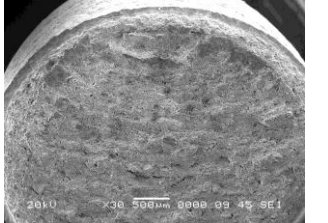
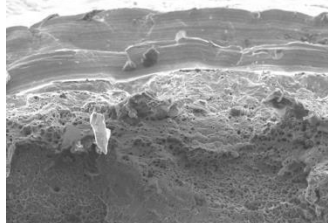
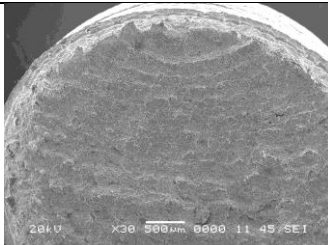
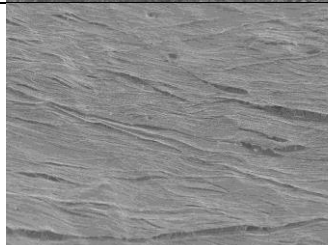

7. Appendix


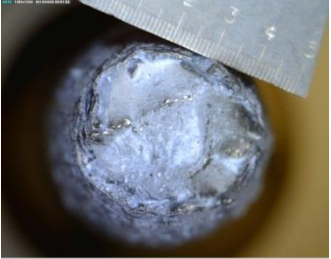
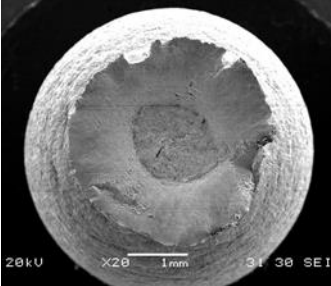
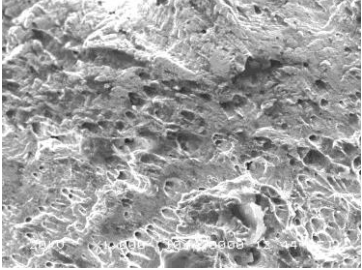
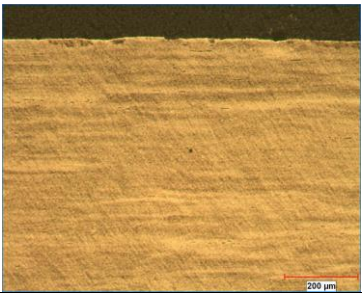

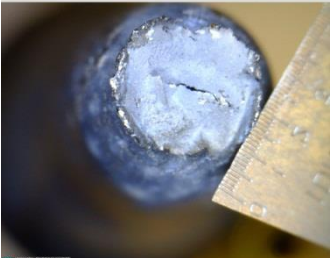
Slow Strain Rate Data

Specimen Number	Process	Environment (9×10^{-7} in/s unless noted)	S _y 0.2% offset ksi (MPa)	S _{ult} ksi (MPa)	Elongation at fracture (%)	Reduction in area (%)	Time to Failure (h)
B1	B1 hardened	Lab Air	73.6 (507.5)	97.9 (675.3)	41.4	68.6	157.00
B2	B1 hardened	ASTM seawater	75.6 (521.2)	98.7 (680.4)	40.1	61.6	151.22
B3	B1 hardened	ASTM seawater	76.3 (526.1)	98.9 (681.7)	39.1	56.8	149.23
B4	B1 hardened	Cathodic Protection in ASTM seawater	75.9 (523.3)	98.3 (678.1)	36.2	47.6	137.98
B5	B1 hardened	Cathodic Protection in ASTM seawater	72.4 (499.2)	96.1 (662.5)	42.3	58.8	159.70
B8	B1 hardened	Cathodic Protection in ASTM seawater	73.7 (508.1)	96.8 (667.4)	36.3	54.1	138.33
B6 Notched	B1 hardened	ASTM seawater	73.8 (508.8)	95.8 (660.7)	25.4	46.9	94.1
B7 Notched	B1 hardened	Lab Air	72.9 (502.6)	97.2 (670.2)	30.1	47.0	111.5
B3NO1	B2 hardened	Lab Air	84.7 (584.0)	108.4 (747.4)	38.1	69.1	145.03
B3NO2	B2 hardened	ASTM seawater	83.7 (577.1)	107.1 (738.4)	40.96	68.2	156.4
B3NO3	B2 hardened	Cathodic Protection in ASTM seawater	82.3 (567.4)	104.2 (718.4)	38.1	66.3	145.9
B3U1	B2 untreated	Lab Air	78.5 (541.2)	100.2 (690.9)	57.61	74.3	218.4
B3U2	B2 untreated	ASTM seawater	77.5 (534.3)	99.3 (684.6)	52.2	70.8	199.2
B3U3	B2 untreated	Cathodic Protection in ASTM seawater	72.7 (501.2)	100.5 (692.9)	50.8	71.9	192.9

Slow Strain Rate Microscopy

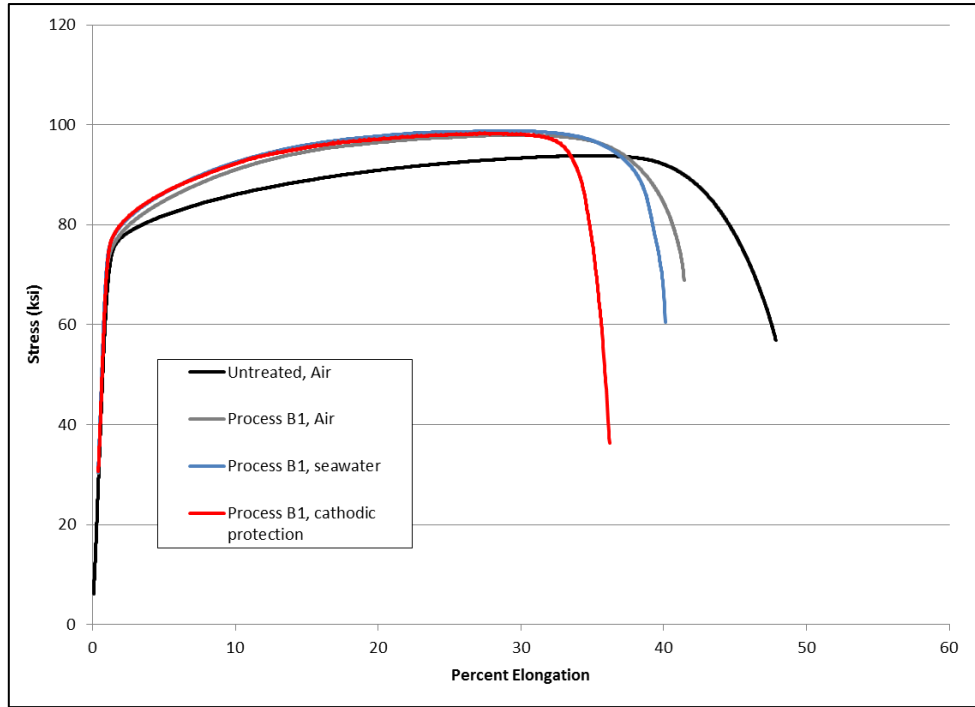
Specimen Number	Environment (9×10^{-7} in/s unless noted)	Fracture Surface	Edge section
B1	Lab Air		 
B2	ASTM seawater		
B3	ASTM seawater		 
B4	Cathodic Protection in ASTM seawater		

B5	Cathodic Protection in ASTM seawater		
B8	Cathodic Protection in ASTM seawater		 
B6 Notched	ASTM seawater		
B7 Notched	Lab Air		
B3NO1	Lab Air		

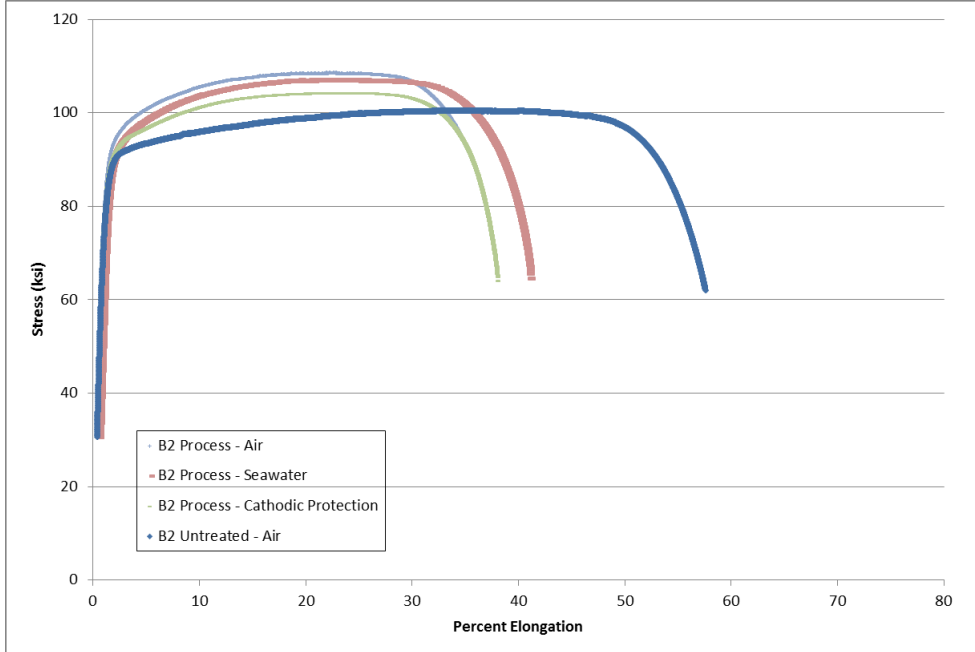
B3NO2	ASTM seawater		
B3NO3	Cathodic Protection in ASTM seawater		
B3U1	Lab Air		 
B3U2	ASTM seawater		
B3U3	Cathodic Protection in ASTM seawater		

Slow Strain Rate Graphs

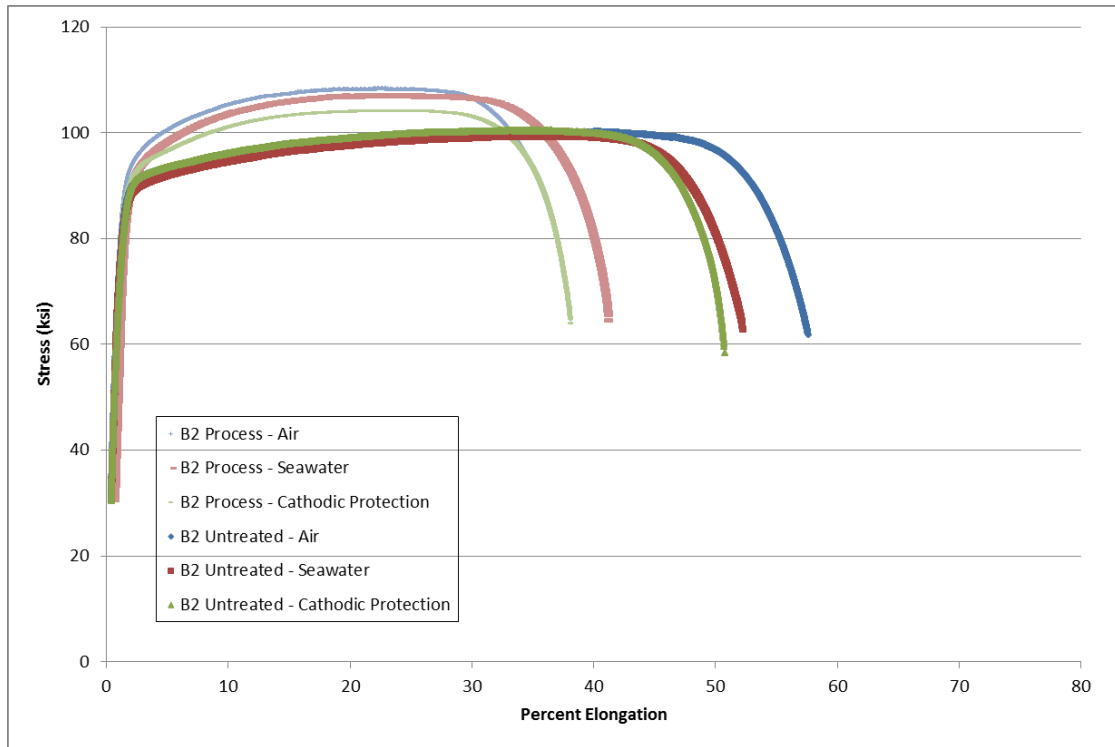
Process B1 (three conditions + untreated)



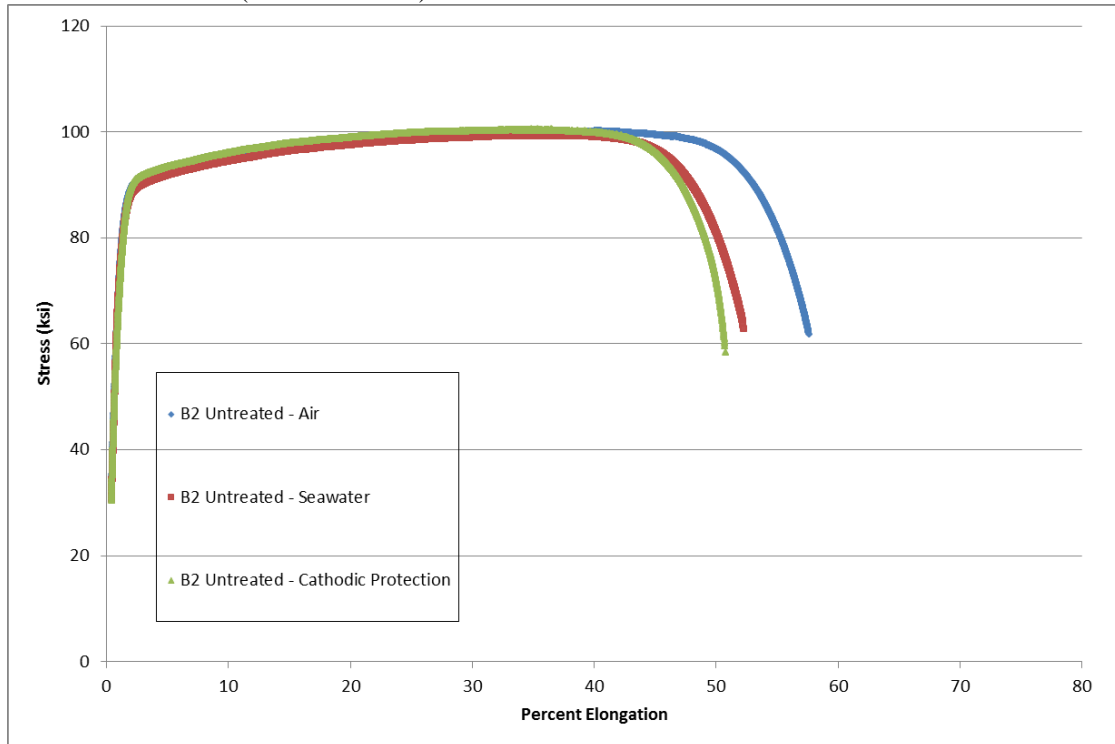
Process B2 (three conditions + untreated)



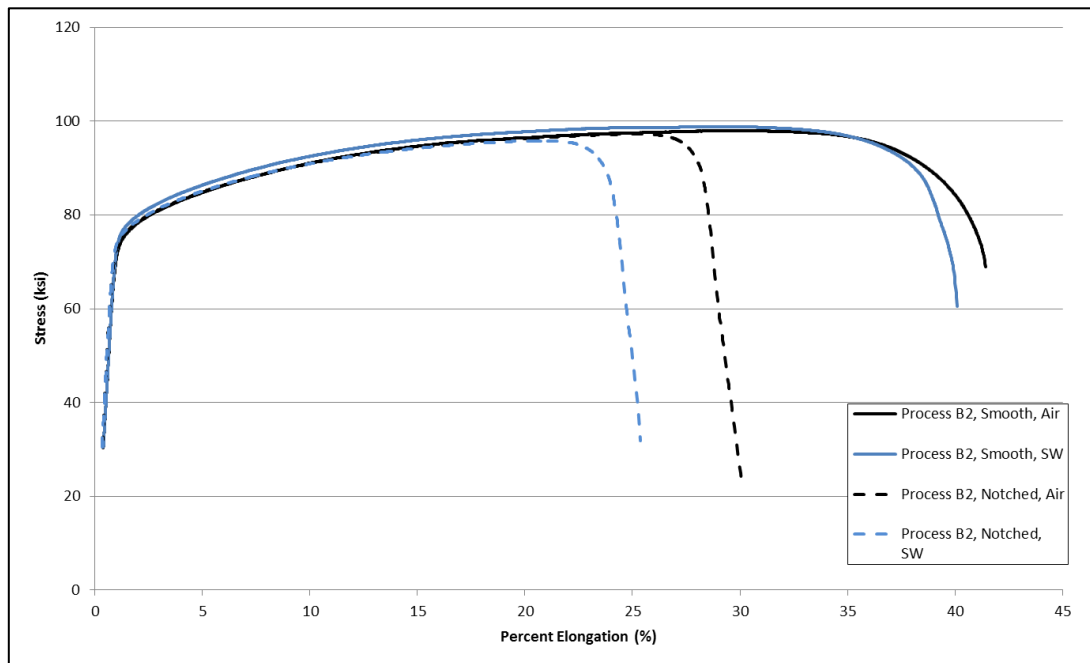
Process B2 treated and untreated (three conditions)



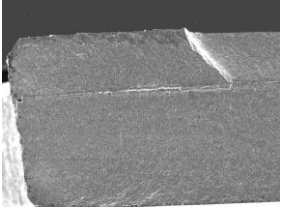
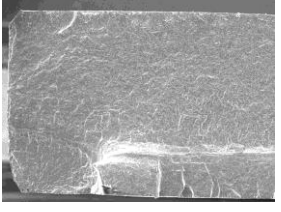
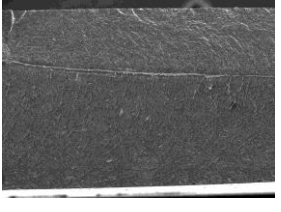
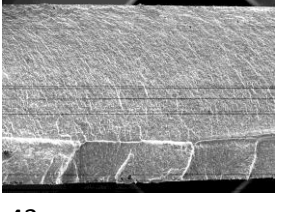
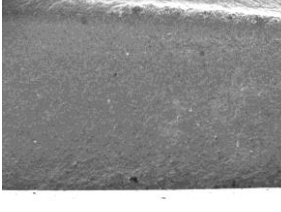
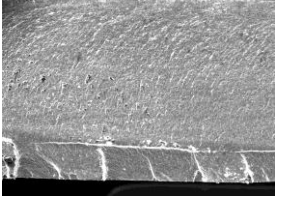
Process B2 untreated (three conditions)

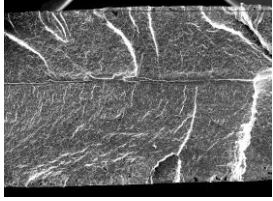
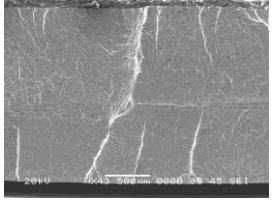
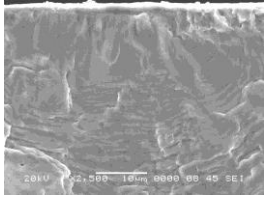

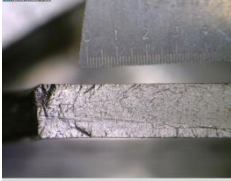
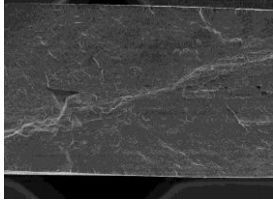
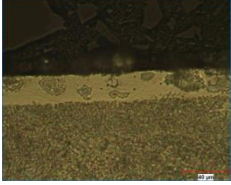

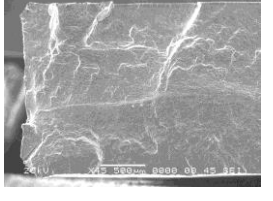



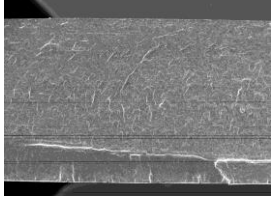

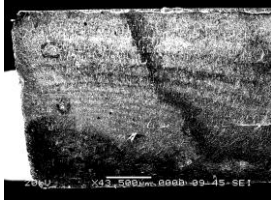

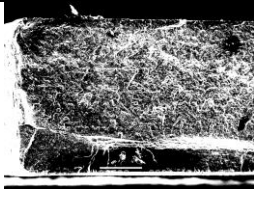
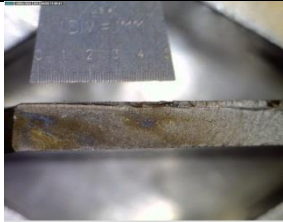
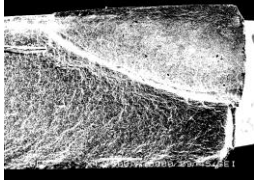

Process B2 Notched samples compared with smooth samples (two conditions)



Fatigue Microscopy

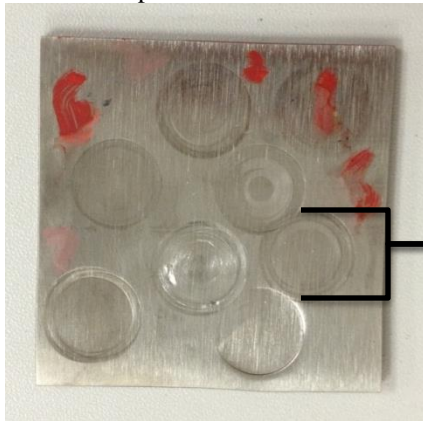
Sample Number	Environment	SEM Fracture Images	Optical Images of the Surface/Etchings
U6	Untreated, Air	 x43	
U7	Untreated, Air	 x43	
U8	Untreated, Air	 x43	
U10	Untreated, Air	 x43	
U11	Untreated, Air	 x43	
U12	Untreated, Air	 x43	

U13	Untreated, Air		
U14	Untreated, Air		
B2	Treated, Air		 
B4	Treated, Air		 
B6	Treated, Air		

B7	Treated, Air		
BS1	Treated, SW		
BS2	Treated, SW		
BS3	Treated, SW		

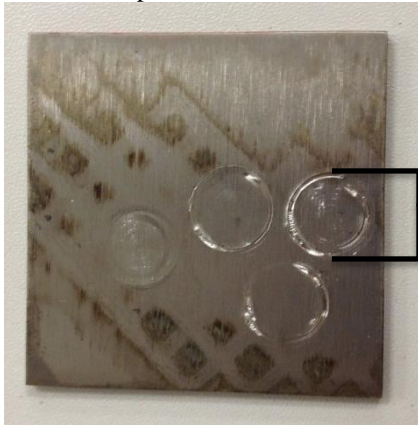
Galling Coupons

Treated Coupon #1



Diameter = 0.5 inches

Treated Coupon #2



Diameter = 0.5 inches